ISSN 1063-7761, Journal of Experimental and Theoretical Physics, 2011, Vol. 112, No. 2, pp. 310–316. © Pleiades Publishing, Inc., 2011.
Original Russian Text © T.V. Perevalov, V.A. Gritsenko, 2011, published in Zhurnal Eksperimental'noi i Teoreticheskoi Fiziki, 2011, Vol. 139, No. 2, pp. 359–366.

ELECTRONIC PROPERTIES OF SOLID

Electronic Structure of TiO_2 Rutile with Oxygen Vacancies: Ab Initio Simulations and Comparison with the Experiment

T. V. Perevalov* and V. A. Gritsenko**

Institute of Semiconductor Physics, Siberian Branch, Russian Academy of Sciences, Novosibirsk, 630090 Russia

** e-mail: timson@isp.nsc.ru*

*** e-mail: grits@isp.nsc.ru*

Received May 7, 2010

Abstract—The electronic structure of TiO_2 rutile with oxygen vacancies, which is a promising insulator, has been analyzed. The ab initio density functional calculations, as well as the comparative analysis of the results obtained in the σ-GGA spin-polarized generalized approximation and those obtained by the σ-GGA + U method with allowance for Coulomb correlations of d electrons titanium atoms in the Hartree–Fock approximation for the Hubbard model, have been performed. It has been found that the effective electron mass in rutile is anisotropic and there are both light ($m_e^* = (0.6–0.8)m_0$, where m_0 is the free-electron mass) and heavy ($m_e^* > 1m_0$) electrons, whereas holes in rutile are only heavy ($m_h^* \geq 2m_0$). It has been shown that the σ-GGA + U method gives a deep occupied level in the band gap and that an oxygen vacancy in rutile is an electron and hole trap.

DOI: 10.1134/S1063776111010158

1. INTRODUCTION

Titanium oxide is crystallized in three modifications: rutile, anatase, and brookite. Rutile is the most widespread and thermodynamically stable crystalline modification. Rutile also attracts attention, because it is structurally and chemically similar to stishovite (SiO_2) and a number of other compounds [1]. The technological importance of rutile stimulated a large number of theoretical [2–13] and experimental [14–20] investigations of its electronic properties.

Compound TiO_2 is important in view of numerous technological applications in catalysis [21] and electrochemistry [22], as a pigment for paints and polymers, in dielectric materials of microelectronics, and in solar elements [23]. Since TiO_2 has a large dielectric constant ($\varepsilon \approx 80$), it is a promising material for microelectronics (the so-called high-k insulator). In particular, TiO_2 is of large interest for potentially using as a subgate insulator in the next generation of metal–insulator–semiconductor silicon devices [24–29]. A high dielectric constant of TiO_2 allows an increase in the thickness of the subgate layer, thus suppressing unacceptably high tunneling leakage currents, which are inevitable in further scaling of integrated circuits [30]. Another important application of TiO_2 as a high-k insulator is its application as an insulator in storage capacitors of SRAM and DRAM devices [31, 32]. The use of TiO_2 leads to an increase in their information capacity owing to a decrease in the area of cells of storage capacitors. In addition, TiO_2 is considered at present as a promising material for resistive energy-independent memory devices [33].

Intrinsic defects in TiO_2 can strongly change its electronic and optical properties. Under usual growth conditions, oxygen-depleted rutile TiO_{2-x} is formed. Consequently, oxygen vacancies and titanium interstitial atoms are dominant intrinsic defects in rutile [34]. However, recent theoretical investigation [35] indicates that the formation of oxygen vacancies is energetically favorable than the introduction of a titanium atom into an interstitial site. Oxygen vacancies can form defect centers serving as electron traps and thus promote charge transfer [26]. High leakage currents constitute one of significant problems for the introduction of high-k insulators in silicon devices. At present, the nature (atomic and electronic structures) of centers responsible for charge transfer in TiO_2 remains unclear [30]. Thus, the study of the electronic structure of rutile, in particular, the determination of the effective masses of electrons and holes, as well as the investigation of the capability of oxygen vacancies to capture charge carriers, i.e., to be involved in conduction is an important aim. Oxygen vacancies in rutile were actively studied both experimentally [36–40] and theoretically [30, 41–52]. The results obtained in this work will be compared to the earlier data.

The aim of this work is to analyze the atomic and electronic structures of an oxygen vacancy in a rutile crystal as the most probable intrinsic effect. The ab initio simulation is performed in the framework of

density functional theory. Electron–electron Coulomb correlations between the *d* electrons of titanium atoms are taken into account in the Hartree–Fock approximation for the Hubbard model [53–55]. The simulation results are compared to the experimental data for rutile and amorphous TiO_2. Various charge states of an oxygen vacancy in rutile are studied and the localization energies of electrons and holes on the oxygen vacancy are calculated.

2. SIMULATION METHOD

The simulation is carried out in the Kohn–Sham density functional theory [56] with the exchange-correlation functional of the generalized gradient approximation in the spin-polarized variant taking into account the Coulomb interaction between 3*d* electrons of titanium atoms in the Hubbard model (σ-GGA + *U*). The calculations are performed with the Quantum-ESPRESSO suite [57]. The Bloch functions of electrons in a crystal are sought in the form of the expansion in plane waves with a cutoff energy of 40 Ry. The potentials of nuclei and core electrons of titanium and oxygen atoms are taken into account in terms of ultrasoft atomic pseudopotentials [58]. The calculations are performed with the GGA pseudopotentials in the Perdew–Burke–Erzerhof parameterization [59]. A value of 3.4 eV for the parameter *U* for the *d* electrons of titanium atoms was obtained using the linear response approximation proposed in [54]. To simulate stoichiometric rutile, as well as oxygen vacancies in it, we used a supercell of 96 atoms created by the $2 \times 2 \times 4$ translation of the unit cell of rutile. The calculations were performed using the uniform $2 \times 2 \times 2$ grid of *k* points in the Brillouin zone. To minimize mechanical stresses in the supercell, the geometry optimization procedure was performed to minimize the force acting on an individual ion below 0.01 eV/Å.

It is known that the direct Coulomb single-site interaction *U* can significantly affect the depth of defect states in the band gap, as well as the charge localization degree. To describe electron correlation more correctly than it was described in the σ-GGA calculations, we used the σ-GGA + *U* method in this work. A similar approach was used in [52]. According to the σ-GGA calculations, oxygen vacancies form shallow electron states near the bottom of the conduction band [35]. According to the calculations performed in [52] by the σ-GGA + *U* method, as well as by the hybrid functional method, oxygen vacancies form deep defect levels in the band gap.

The crystal structure of TiO_2 rutile is described by the simple Brave tetragonal lattice and has the $P4/2mnm$ (D_{4h}^{14}) space symmetry group. The unit cell of rutile contains two TiO_2 formula units. Titanium atoms are six-fold coordinated with oxygen atoms four of which are at a distance of 1.945 Å and two are at a distance of 1.985 Å. The direction of long bonds is [110]. Oxygen atoms are three-fold coordinated with titanium atoms.

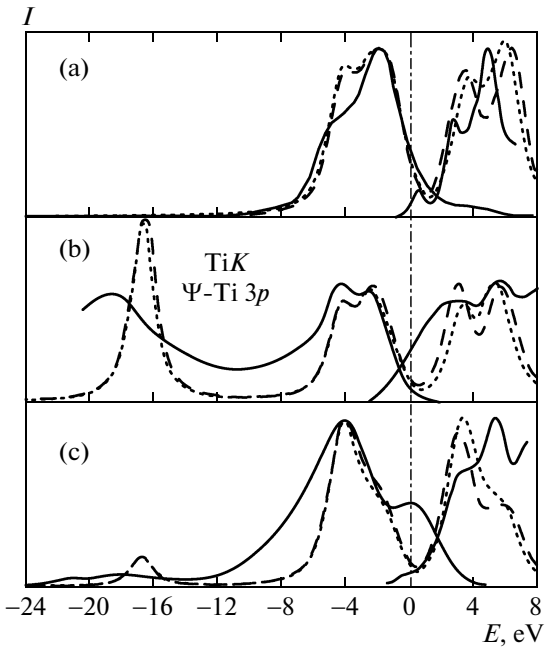

Fig. 1. (Solid lines) Experimental emission and quantum yield spectra (a) O *K*, (b) Ti *K*, and (c) Ti L_{III} of rutile in comparison with the respective spectra of (a) O 2*p*, (b) Ti 3*p*, and (c) Ti 3*d* partial densities of states obtained in the (dashed lines) σ-GGA and (dotted lines) σ-GGA + *U* calculations. The calculated spectra are broadened with the Lorentz function with an FWHM of 0.7 eV.

3. ELECTRONIC STRUCTURE OF PERFECT RUTILE

First, the simulation of the electronic structure of a perfect rutile crystal was performed in two calculation approximations, σ-GGA and σ-GGA + *U*. According to these calculations, rutile is a direct-band insulator with the top of the valence band and the bottom of the conduction band at the Γ point of the Brillouin zone. The band gap E_g is 1.9 eV in the σ-GGA calculations and 2.2 eV in the σ-GGA + *U* calculations. The experimental E_g values for rutile are in the range of 3.0–3.2 eV [14–17, 60]. The discrepancy between the experimental and calculated values is attributed to the systematic underestimation of E_g by the density functional methods.

Figure 1 shows the experimental O *K*, Ti L_{III}, and Ti *K* spectra and X-ray emission and quantum-yield spectra for rutile (taken from [15]), as well as the corresponding calculated partial densities of states given in one energy scale. The energies are measured from the top of the valence band. The Ti L_{III}spectra exhibit the transitions from the 4*s* and 3*d* states of titanium in the valence band to the Ti 2*p* levels. The Ti *K* spectra exhibit the transitions from the Ti 3*p* states to the Ti 2*s*

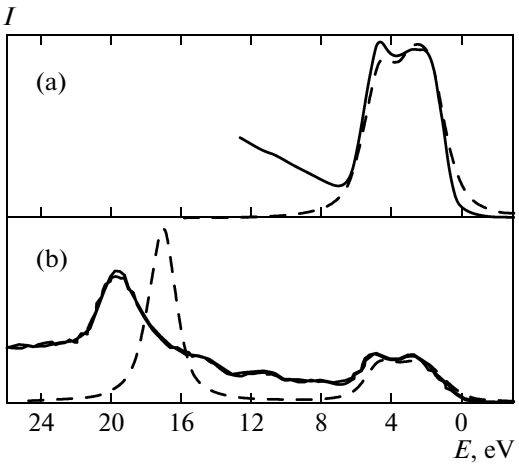

Fig. 2. (Solid lines) Experimental (a) ultraviolet photoelectron spectrum with an excitation energy of $h\nu = 47$ eV and (b) X-ray photoelectron spectrum with $h\nu = 1486.6$ eV of the valence band of TiO_2 rutile in comparison with (dashed lines) the respective calculated spectra. The calculated spectra are broadened with the Lorentz function with an FWHM of 0.7 eV.

level. The O K emission spectra are observed when electrons transit from the O 2p levels to the O 1s levels. To the energy dependence of the transition matrix elements, the X-ray emission spectra, as well as the quantum-yield spectra, reflect the partial densities of states. Since the calculated spectra of the partial densities of states of Ti 4s make a negligibly small contribution to the formation of the valence band as compared to the Ti 3d spectra, the experimental Ti L_{III}spectra in Fig. 1 are compared only to the calculated Ti 3d spectra.

The spectra of the valence band of rutile obtained in both calculation approximations are almost the same, whereas there are noticeable discrepancies for the states of the conduction band. In addition, the positions and number of peaks in the calculated and experimental spectra are in satisfactory qualitative agreement. Agreement between the calculated Ti 3p spectra and Ti K emission spectrum is observed only for the upper valence band and conduction band. The calculated peaks in the Ti 3p spectra in the lower valence band are higher than the respective experimental peaks. A similar discrepancy with the experimental data was observed in SiO_2 and Si_3N_4 [61], as well as in Al_2O_3 [62]. The calculated spectrum of the partial densities of states of Ti 3d does not describe the upper peak of the valence band in the experimental Ti L_{III} spectrum. The upper peak of the valence band in the experimental Si L spectra in SiO_2 and Si_3N_4 is due to the 3d orbitals of silicon and nonlocal (two-center) transitions [61].

Table 1. Calculated minimum and maximum effective masses of electrons m_e^* and holes m_h^* in rutile with the indication of the corresponding directions in the Brillouin zone

Calculation type	Effective mass	
	m_e^*/m_0	m_h^*/m_0
σ-GGa	0.6 ($\Gamma \longrightarrow Z$) 1.2 ($\Gamma \longrightarrow M$)	2.6 ($\Gamma \longrightarrow X$) 4.8 ($\Gamma \longrightarrow Z$)
σ-GGa + U	0.8 ($\Gamma \longrightarrow Z$) 12 ($\Gamma \longrightarrow M$)	2.0 ($\Gamma \longrightarrow X, M$) 3.4 ($\Gamma \longrightarrow Z$)

Figure 2 shows the experimental ultraviolet photoelectron spectra [63] and X-ray photoelectron spectra [64] of the rutile single crystal in comparison with the respective calculated spectra. The energy is measured from the top of the valence band. The calculated ultraviolet and X-ray photoelectron spectra are obtained by summing the partial densities of states of valence orbitals with weight factors, which are equal to the corresponding photoionization cross sections taken from [65]. Since the calculation models used in this work provide the identical spectra of the partial densities of states of the valence band (see Fig. 1), the photoelectron spectra in Fig. 2 are calculated only in the σ-GGA + U approximation. It is seen that the relative intensities of the main peaks of the calculated ultraviolet and X-ray photoelectron spectra of rutile are in agreement with the relative intensities of the peaks of the respective experimental spectra. The main contribution to the calculated ultraviolet photoelectron spectra (see Fig. 2a) comes from the O 2p orbitals. Two bands corresponding to photoemission from the O 2s and Ti 3p states are seen in the X-ray photoelectron spectra in Fig. 2b. The inconsistency in the positions of main peaks is likely due to the underestimated calculated widths of the upper and lower valence bands, which are characteristic of the density-functional calculations. The difference between the widths of the experimental and respective calculated peaks can also be caused by the finite lifetime of the hole on the core levels, which leads to the broadening of the experimental peaks. The inclusion of the processes responsible for the broadening of the peak (e.g., Auger processes) requires a much more complex model.

Thus, agreement between the calculated and respective experimental spectra indicates that the performed band calculations provide a qualitatively correct pattern of the electronic structure of rutile.

Table 1 presents the calculated minimum and maximum effective masses of electrons m_e^* and holes m_h^* in the rutile crystal with the indication of the corresponding directions in the Brillouin zone. The effective masses were calculated by the quadratic-function approximation of the calculated dispersion law $E(\mathbf{k})$ near the top of the valence band and the bottom of the conduction band using the formula

$$m_{\alpha\beta}^{-1} = \frac{1}{\hbar^2}\frac{\partial^2 E(\mathbf{k})}{\partial k_\alpha \partial k_\beta}. \quad (1)$$

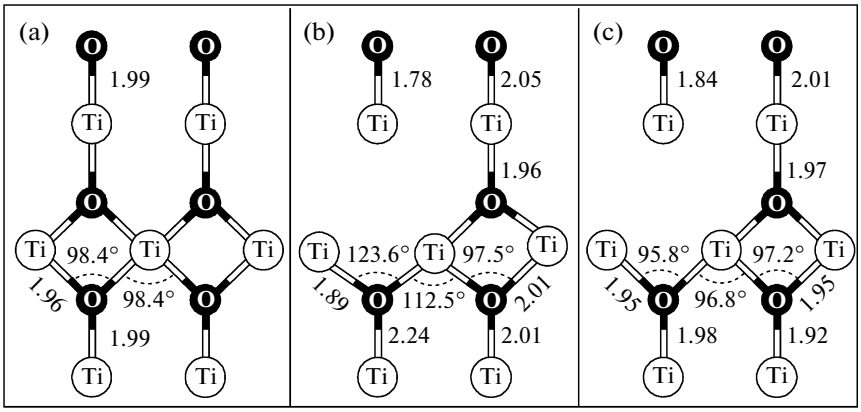

Fig. 3. Optimized positions of Ti and O atoms in the (110) plane in (a) perfect rutile, as well as in rutile with an oxygen vacancy calculated in the (b) σ-GGA and (c) σ-GGA + *U* approximations. The interatomic distances are given in angstroms.

There are both heavy electrons (in the $\Gamma \longrightarrow M$ direction) and light electrons (in the $\Gamma \longrightarrow Z$ direction) in rutile. The effective electron mass in the rutile crystal obtained from the experimental data has a wide spread of the values: $m_e^* = 0.5m_0$ [66], $m_e^* = 3m_0$ [67], and $m_e^* = 8.4m_0$ [16] (where m_0 is the free-electron mass). The experimental effective masses of holes in TiO_2 are not reported. According to the calculations, holes in the rutile crystal are heavy, $m_h^* \geq 2.0m_0$. It is seen that the σ-GGA + *U* calculations provide larger effective electron masses and smaller effective hole masses. The effective electron mass in the $\Gamma \longrightarrow M$ direction increases by an order of magnitude. The effective hole masses decrease slightly.

4. ELECTRONIC STRUCTURE OF OXYGEN VACANCIES IN RUTILE

Figure 3a shows the positions of Ti and O atoms in the (110) plane of the rutile crystal. Figures 3b and 3c show the equilibrium positions of the same atoms after the removal of one oxygen atom. It is seen that shifts caused by the oxygen vacancy change the lengths of the Ti–O bonds, but do not change the shape of the local arrangement of the nearest and next-to-nearest atoms. The removal of the oxygen atom induces the shift of surrounding Ti atoms in the (110) plane in the direction from the vacancy by 0.28–0.29 Å in the σ-GGA calculation and by 0.04–0.17 Å in the σ-GGA + *U* calculation. The result obtained for relaxation in the σ-GGA + *U* calculation almost coincides with the results calculated in [35, 51]. The shift of Ti atoms from the vacancy is explained by the fact that the removal of the oxygen ion increases the repulsion between the Ti ions nearest to the vacancy. Such a relaxation of the positions of Ti atoms effectively screens the positive charge *q* of the oxygen vacancy. The Löwdin population analysis indicates that $q = 1.62e$ on Ti atoms far from the vacancy and $q = 1.54e$ on three Ti atoms nearest to the vacancy in the σ-GGA calculation and $q = 1.62e$ and $q = 1.55e$, respectively, in the σ-GGA + *U* calculation. A smaller change in the charge on the Ti atoms nearest to the vacancy in the σ-GGA + *U* calculations explains a weaker relaxation of the positions of atoms (see Figs. 3b, 3c).

Figure 4 shows the calculated dispersion spectra $E(\mathbf{k})$ of the energy bands for perfect rutile, as well as for rutile with oxygen vacancies. The energy is measured from the top of the valence band. The presence of the oxygen vacancy in rutile leads to the appearance of a defect level in its band gap. This level is occupied by two electrons. The defect level in the σ-GGA simulation almost coincides with the bottom of the conduction band (see Fig. 4b), whereas the inclusion of the Hartree–Fock correction in the GGA calculation provides the defect level that is at a distance of 0.6 eV from the bottom of the conduction band (see Fig. 4c). Analysis of the calculated partial densities of states indicates that the defect level is almost completely formed from the 3*d* states of titanium atoms with the admixture of the 2*p* states of oxygen. An almost flat curve of the dispersion law for the defect level indicates strong localization in the real space.

Thus, the obtained results imply that the oxygen vacancy in rutile serves as a deep donor. The existence of deep levels is in agreement with the experimental data for rutile [38, 68], according to which oxygen vacancies form electron-occupied levels in the band gap about 1 eV below the bottom of the conduction band. Furthermore, a deep occupied level in the band gap of rutile, which is due to the presence of oxygen vacancies, was obtained in theoretical works [50, 52]. The position of the defect level with respect to the top of the valence band and the bottom of the conduction band obtained in this work is apparently underestimated in view of the underestimation of the width of the band gap.

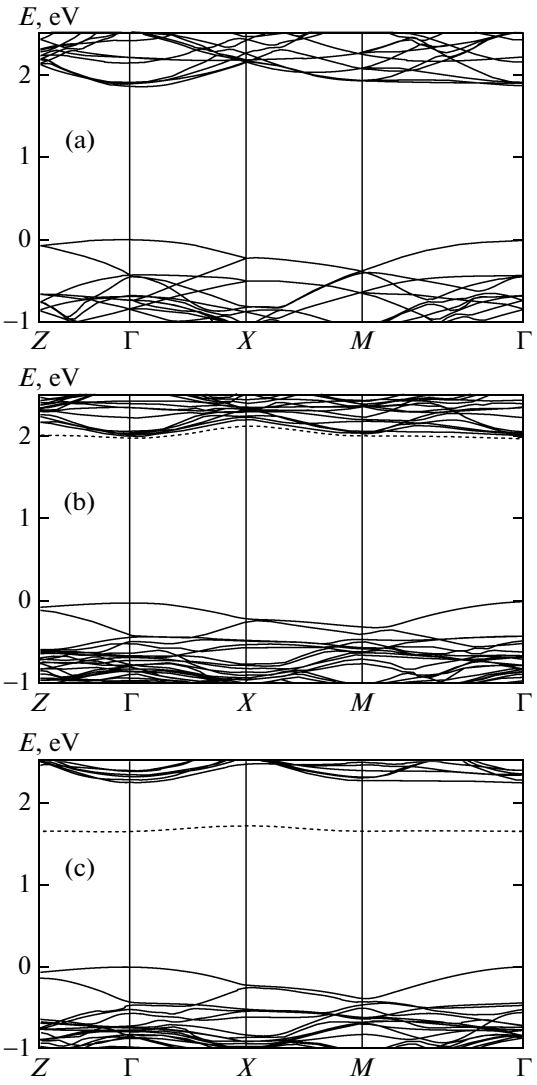

Fig. 4. Calculated band structures of rutile constructed along the high-symmetry directions of the Brillouin zone for (a) perfect rutile, as well as for rutile with the oxygen vacancy in the (b) σ-GGA and (c) σ-GGA + U approximations. The dashed line indicates the level of the oxygen vacancy.

Figure 5 shows the calculated ultraviolet photoelectron spectrum of rutile with a periodic intrinsic effect, which is an oxygen vacancy, in comparison with the experimental ultraviolet photoelectron spectrum of the oxygen-depleted TiO_2 crystal [63]. The experimental spectrum was obtained on the rutile crystal irradiated by Ar^+ ions with a defect density of 10^{17}–10^{18} cm^{-3}. The energy is measured from the top of the valence band. The calculated ultraviolet photoelectron spectrum exhibits a peak, which is due to the presence of oxygen vacancies, at 1.6 eV above the top of the valence band; it is obviously associated with the 2.8-eV experimental peak. This result indicates the high density of neutral oxygen vacancies in the rutile crystal irradiated by argon ions.

Table 2. Calculated localization energies of electrons and holes on an oxygen vacancy in rutile

Calculation type	Localization energy	
	$\Delta\varepsilon^e$, eV	$\Delta\varepsilon^h$, eV
σ-GGa	0	1.9
σ-GGa + U	0.1	2.3

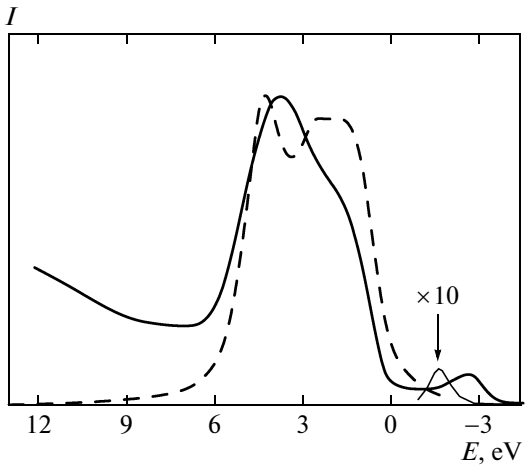

Fig. 5. (Solid lines) Experimental ultraviolet photoelectron spectrum with $h\nu$ = 47 eV of rutile bombarded by argon [63] in comparison with (dashed lines) the calculated ultraviolet photoelectron spectrum of rutile with an oxygen vacancy. The calculated spectra are broadened with the Lorentz function with an FWHM of 0.4 eV.

To analyze the possibility of the capture of an electron/hole on the oxygen vacancy in rutile, one electron is added to/removed from the calculated structures. To ensure the electroneutrality of the system under the addition of an excess charge in the used calculation model, a uniform background compensating charge is introduced. The charge localization energy is estimated as the difference between the electron affinity and ionization energy for defect and perfect cells [69]:

$$\Delta\varepsilon^{e/h} = (E^{q=-1/+1}_{\text{perfect}} - E^{q=0}_{\text{perfect}}) - (E^{q=-1/+1}_{\text{defect}} - E^{q=0}_{\text{defect}}). \quad (2)$$

It was found that the capture of both an electron and a hole onto the oxygen vacancy in rutile is energetically profitable. Table 2 presents the calculated localization energies of electrons and holes on the oxygen vacancy. It is worth noting that the density functional calculations fundamentally provide the incorrect position of the bottom of the conduction band and, correspondingly, tend to underestimate the electron localization degree. An error associated with the erroneous position of the edges of the bands depends on the type of the defect and cannot be estimated without a careful calibration using the experimental data. Thus, accord-

ing to the performed calculations, the oxygen vacancy in rutile can serve as a localization center (trap) for both an electron and a hole. Therefore, the presence of oxygen vacancies in rutile can explain a high electric conductivity of rutile.

5. CONCLUSIONS

The atomic and electronic structures of TiO_2 in the rutile modification, which is a promising insulator, have been analyzed in detail by the ab initio methods. The comparative analysis of the results obtained in the σ-GGA and σ-GGA + U calculations has been performed.

The Coulomb interaction is taken into account in the static approximation in the Hubbard model to more correctly describe electron–electron correlations between 3d electrons of the titanium atom. Agreement between the calculated and respective experimental data indicates that the used theoretical model satisfactorily describes the main features of the X-ray and photoelectron spectra of the valence band.

The σ-GGA + U calculations provide a wider band gap as compared to the σ-GGA calculations, but it is yet much narrower than the experimental value. Furthermore, the σ-GGA + U calculations provide heavier electrons and lighter holes as compared to the σ-GGA calculations. Both calculation methods indicate the presence of both light ($m_e^* = (0.6–0.8)m_0$) and heavy ($m_e^* > 1m_0$) electrons and only heavy holes ($m_h^* \geq 2m_0$). The electron component of the current in rutile can prevail over the hole component in view of the higher mobility of electrons.

The simulation of the electronic structure of an oxygen vacancy, which is the most widespread intrinsic effect in TiO_2 rutile, indicates that the Hartree–Fock correction and the Coulomb interaction U for Ti 3d electrons strongly affect the depth of the defect states in the band gap. The defect level in the σ-GGA calculations almost coincides with the bottom of the conduction band, whereas the σ-GGA + U calculation provides a deep occupied level at 0.6 eV from the bottom of the conduction band.

Analysis of the localization of charge carriers on defects in rutile indicates that the capture of both an electron and a hole onto the oxygen vacancy is energetically profitable. This means that oxygen vacancies in rutile can capture both electrons and holes and, consequently, serve as electron and hole traps, respectively. The inaccuracy of this calculation is in the systematic underestimation of the band gap by the density functional methods; as a result, the localization energy is underestimated. The results imply that high leakage currents in rutile can be attributed to oxygen vacancies.

ACKNOWLEDGMENTS

This work was supported by the Russian Foundation for Basic Research (project no. 10-07-00531-a) and by the Siberian Branch, Russian Academy of Sciences (integration project no. 70). The work was performed in part at the NKS-160 Supercomputer Center, Siberian Branch, Russian Academy of Sciences.

REFERENCES

1. R. W. G. Wyckoff, *Crystal Structures* (Wiley, New York, United States, 1974).
2. H. M. Lawler, J. J. Rehr, F. Vila, S. D. Dalosto, E. L. Shirley, and Z. H. Levine, Phys. Rev. B: Condens. Matter **78**, 205 108 (2008).
3. P. K. Schelling, N. Yu, and J. W. Halley, Phys. Rev. B: Condens. Matter **58** (3), 1279 (1998).
4. A. F. Fahmi, C. Minot, B. Silvi, and M. Causa, Phys. Rev. B: Condens. Matter **47** (18), 11 717 (1993).
5. L. B. Lin, S. D. Mo, and D. L. Lin, J. Phys. Chem. Solids **54**, 8 (1993).
6. S. D. Mo and W. Y. Ching, Phys. Rev. B: Condens. Matter **51**, 13 023 (1995).
7. K. M. Glassford and J. R. Chelikowsky, Phys. Rev. B: Condens. Matter **46** (3), 1284 (1992).
8. K. M. Glassford and J. R. Chelikowsky, Phys. Rev. B: Condens. Matter **45**, 3874 (1992).
9. B. Poumellect, P. J. Durham, and G. Y. Guo, J. Phys.: Condens. Matter **3**, 8195 (1991).
10. P. Reinhardt, B. A. Heb, and M. Causa, Int. J. Quantum Chem. **58**, 297 (1996).
11. M. A. Khan, A. Kotani, and J. C. Parlebas, J. Phys.: Condens. Matter **3**, 1763 (1991).
12. T. V. Perevalov and V. A. Gritsenko, Usp. Fiz. Nauk **180** (6), 587 (2010) [Phys.—Usp. **53** (6), 561 (2010)].
13. V. A. Gritsenko and T. V. Perevalov, in *Dielectrics in Microelectronics*, Ed. by A. L. Aseev (Siberian Branch of the Russian Academy of Science, Novosibirsk, 2010), p. 258 [in Russian].
14. A. Amtout and R. Leonelli, Phys. Rev. B: Condens. Matter **51** (11), 6842 (1995).
15. D. Fischer, Phys. Rev. B: Solid State **5** (11), 4219 (1972).
16. J. Pascual, J. Camassel, and H. Mathieu, Phys. Rev. B: Condens. Matter **18**, 5606 (1978).
17. C. Ting, S. Chen, and D. Liu, J. Appl. Phys. **88**, 4628 (2000).
18. J. B. Goodenough, Prog. Solid State Chem. **5**, 145 (1971).
19. V. E. Henrich, Rep. Prog. Phys. **48**, 1481 (1985).
20. M. Mosaddeq-ur-Rahman, G. Yu, T. Soga, T. Jimbo, H. Ebisu, and M. Umeno, J. Appl. Phys. **88**, 4634 (2000).
21. S. J. Tauster, S. C. Fung, and R. L. Garten, J. Am. Chem. Soc. **100**, 170 (1978).
22. D. J. Dwyer, S. D. Cameron, and J. Gland, Surf. Sci. **159**, 430 (1985).
23. S. Sato and J. M. White, J. Phys. Chem. **85**, 592 (1981).

24. J. Yan, D. C. Gilmer, S. A. Campbell, W. L. Gladfelter, and P. G. Schmid, J. Vac. Sci. Technol., B: Microelectron. Nanometer Struct.—Process., Meas., Phenom. **14**, 1706 (1996).
25. H.-S. Kim, D. C. Gilmer, S. A. Campbell, and D. L. Polla, Appl. Phys. Lett. **69**, 3860 (1996).
26. S. A. Campbell, D. C. Gilmer, X.-C. Wang, M. T. Hsieh, H.-S. Kim, W. L. Gladfelter, and J. Yan, IEEE Trans. Electron Devices **44**, 104 (1997).
27. H.-S. Kim, S. A. Campbell, and D. C. Gilmer, IEEE Electron Device Lett. **18**, 465 (1997).
28. H.-S. Kim, S. A. Campbell, D. C. Gilmer, V. Kaushik, J. Conner, L. Prabhu, and A. Anderson, J. Appl. Phys. **85**, 3278 (1999).
29. C. K. Maiti, S. K. Samanta, G. K. Dalapati, S. K. Nandi, and S. Chatterjee, Microelectron. Eng. **72**, 253 (2004).
30. A. I. Kingon, J.-P. Maria, and S. K. Streiffer, Nature (London) **406**, 1032 (2000).
31. J. Robertson, Eur. Phys. J.: Appl. Phys. **28**, 265 (2004).
32. S. K. Kim, W.-D. Kim, K.-M. Kim, C. S. Hwang, and J. Jeong, Appl. Phys. Lett. **85**, 4112 (2004).
33. V. K. Yarmarkin, S. G. Shul'man, and V. V. Lemanov, Fiz. Tverd. Tela **50**, 1767 (2008) [Phys. Solid State **50**, 1847 (2008)].
34. K. Hoshino, N. L. Peterson, and C. L. Wiley, J. Phys. Chem. Solids **46**, 1397 (1985).
35. E. Cho, S. Han, H.-S. Ahn, K.-R. Lee, S. K. Kim, and C. S. Hwang, Phys. Rev. B: Condens. Matter **73**, 193202 (2006).
36. V. E. Henrich, G. Dresselhaus, and H. J. Zeiger, Phys. Rev. Lett. **36**, 1335 (1976).
37. R. H. Tait and R. V. Kasowski, Phys. Rev. B: Condens. Matter **20**, 5178 (1979).
38. V. E. Henrich and R. L. Kurtz, Phys. Rev. B: Condens. Matter **23**, 6280 (1981).
39. M. A. Henderson, Surf. Sci. **400**, 203 (1998).
40. U. Diebold, Surf. Sci. Rep. **48**, 53 (2003).
41. S. Munnix and M. Schmeits, Phys. Rev. B: Condens. Matter **31**, 3369 (1985).
42. M. Ramamoorthy, R. D. King-Smith, and D. Vanderbilt, Phys. Rev. B: Condens. Matter **49**, 7709 (1994).
43. N. Yu and J. W. Halley, Phys. Rev. B: Condens. Matter **51**, 4768 (1995).
44. P. J. D. Lindan, N. M. Harrison, M. J. Gillan, and J. A. White, Phys. Rev. B: Condens. Matter **55**, 15919 (1997).
45. T. Bredow and G. Pacchioni, Chem. Phys. Lett. **355**, 417 (2002).
46. J. He and S. B. Sinnott, J. Am. Ceram. Soc. **88**, 737 (2005).
47. V. I. Anisimov, M. A. Korotin, I. A. Nekrasov, A. S. Mylnikova, A. V. Lukoyanov, J. L. Wang, and Z. Zeng, J. Phys.: Condens. Matter **18**, 1695 (2006).
48. H. Iddir, S. Ögüt, P. Zapol, and N. D. Browning, Phys. Rev. B: Condens. Matter **75**, 073 203 (2007).
49. C. D. Valentin, G. Pacchioni, and A. Selloni, Phys. Rev. Lett. **97**, 166 803 (2006).
50. M. M. Islam, T. Bredow, and A. Cerson, Phys. Rev. B: Condens. Matter **76**, 045 217 (2007).
51. L. Liborio and N. Harrison, Phys. Rev. B: Condens. Matter **77**, 104 104 (2008).
52. G. Mattioli, F. Filippone, P. Alippi, and A. A. Bonapasta, Phys. Rev. B: Condens. Matter **78**, 241 201 (2008).
53. V. I. Anisimov, F. Aryasetiawan, and A. I. Liechtenstein, J. Phys.: Condens. Matter **9**, 767 (1997).
54. M. Cococcioni and S. de Gironcoli, Phys. Rev. B: Condens. Matter **71**, 035 105 (2005).
55. H. J. Kulik, M. Cococcioni, D. A. Scherlis, and N. Marzari, Phys. Rev. Lett. **97**, 103 001 (2006).
56. W. Kohn and L. Sham, Phys. Rev. Sect. A **140**, 1133 (1965).
57. S. Baroni, A. Dal Corso, S. de Gironcoli, P. Giannozzi, P. Cavazzoni, G. Balladio, S. Scandolo, G. Chiarotti, P. Focker, A. Pasquarello, K. Laasonen, A. Trave, R. Car, N. Marzari, and A. Kokalj, http://www.quantum-espresso.org/.
58. D. Vanderbilt, Phys. Rev. B: Condens. Matter **41**, 7892 (1990).
59. J. P. Perdew, K. Burke, and M. Ernzerhof, Phys. Rev. Lett. **77**, 3865 (1996).
60. S. Yamamoto, T. Sumita, Sugiharuto, A. Miyashita, and H. Naramoto, Thin Solid Films **401**, 88 (2001).
61. V. A. Gritsenko, Yu. N. Novikov, V. A. Shaposhnikov, and Yu. N. Morokov, Fiz. Tekh. Poluprovodn. (St. Petersburg) **35** (9), 1041 (2001) [Semiconductors **35** (9), 997 (2001)].
62. T. V. Perevalov, A. V. Shaposhnikov, V. A. Gritsenko, H. Wong, J. H. Han, and C. W. Kim, Pis'ma Zh. Eksp. Teor. Fiz. **85** (3), 197 (2007) [JETP Lett. **85** (3), 165 (2007)].
63. Z. Zhang, S. P. Jeng, and V. E. Henrich, Phys. Rev. B: Condens. Matter **43**, 12 004 (1991).
64. S. P. Kowalczyk, F. R. McFeely, L. Ley, V. T. Gritsyna, and D. A. Shirley, Solid State Commun. **23**, 161 (1977).
65. J.-J. Yeh, *Atomic Calculation of Photoionization Cross-Section and Asymmetry Parameters* (Gordon and Breach, Amsterdam, The Netherlands, 1993).
66. V. Mikhelashvili and G. Eisentein, J. Appl. Phys. **89**, 3256 (2001).
67. J. Pascual, J. Camassel, and H. Mathieu, Phys. Rev. Lett. **39**, 1490 (1977).
68. D. C. Cronemeyer, Phys. Rev. **113**, 1222 (1959).
69. A. X. Chu and W. B. Fowler, Phys. Rev. B: Condens. Matter **41**, 5061 (1990).

Translated by R. Tyapaev